Size and Weight Reduction of an In-wheel Axial-gap Motor Using Ferrite Permanent Magnets for Electric Commuter Cars

T. Takahashi[1], M. Takemoto[1], S. Ogasawara[1], W. Hino[2], and K. Takezaki[2]
[1] Hokkaido University, Graduate School of Information Science and Technology, Sapporo 060-0814, Japan
[2] Dynax Corporation, Tomakomai 066-8585, Japan
E-mail: takahashi@sfc.ssi.ist.hokudai.ac.jp

Abstract — In-wheel type permanent magnet synchronous motors for electric commuter cars are required to be compact and light to use limited wheel space effectively and reduce unspringing weight. Therefore, our previous papers presented a low-cost in-wheel axial-gap motor that uses ferrite permanent magnets. This motor adopted an open slot structure to reduce production costs. However, to achieve further size and weight reduction, we examine here in detail the adoption of a semi-closed slot structure instead of an open slot structure. Experimental results show that the semi-closed slot structure is effective in realizing size and weight reduction.

I. INTRODUCTION

Small electric vehicles known as electric commuter cars, which are used for commuting and traveling short distances within cities, are being actively studied by researchers and industrial engineers [1]-[3]. Because of the compact size of these vehicles, the adoption of an in-wheel motor [2]-[4] is desirable for effective use of limited interior space. In addition, conventional traction motors for electric vehicles typically use powerful rare-earth permanent magnets (PMs) to generate large torques [5][6]. However, it is difficult to use such high-cost PMs in the in-wheel motors of electric commuter cars because the production budget is necessarily lower than that for large electric vehicles. Accordingly, it is very important to develop a low-cost in-wheel motor that does not use rare-earth PMs in order to make electric commuter cars more affordable and widespread.

Consequently, our research team has proposed an axial-gap-type in-wheel motor for electric commuter cars that uses ferrite PMs [7]-[9]. In general, torque is decreased by changing from rare-earth PMs to ferrite PMs because the residual magnetic flux density of the latter is only about 30% that of the former. Therefore, in the proposed motor, we adopt an axial-gap configuration that can achieve high torque density in the flat shape required for an in-wheel motor [10]-[15]. Moreover, a coreless rotor structure is used to increase magnetic torque and efficiency. The proposed motor is also equipped with a reduction gearbox on the inner side of the stator to utilize limited wheel space effectively.

In previous papers, we reported on the operational characteristics of the proposed motor with results of experiments on 5-kW and 10-kW prototypes [7]-[9]. In the examinations, an open slot structure is adopted for the stator in order to reduce production costs. It was shown that the proposed motor could satisfy the demands of an in-wheel motor for electric commuter cars, despite using ferrite PMs.

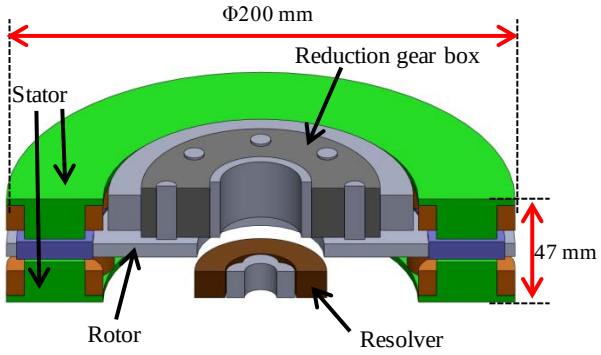

(a) Cross-sectional view

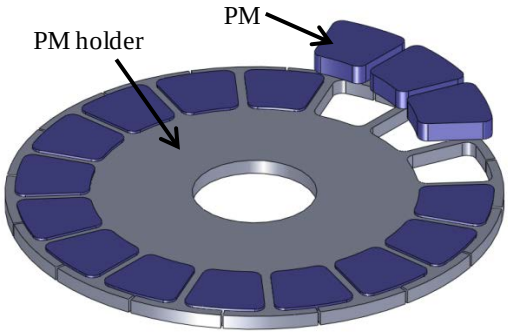

(b) Rotor

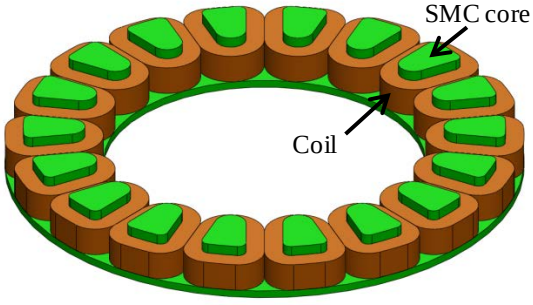

(c) Stator

Fig. 1. Outline of proposed ferrite magnet in-wheel axial-gap motor with open slot structure based on previous examinations. (open slot model (A)).

TABLE I
SPECIFICATIONS AND TARGET VALUE OF 3-KW MOTOR

Number of poles	16
Number of slots	18
Maximum output	3.0 kW
Rated output	2.0 kW
Maximum torque	12.0 Nm
Base speed	2400 rpm
Maximum speed	5000 rpm
Max. current density	10 A/mm^2
Diameter	200 mm
Motor length	less than 40 mm
Motor Weight	less than 5.5 kg

Our research team intends to develop a new 3-kW small-size motor. In order to achieve further size and weight reduction compared with the previously proposed motor, we examine afresh and in detail the adoption of a semi-closed slot structure instead of an open slot structure. Our experimental results show that the semi-closed slot structure is effective in realizing size and weight reduction.

II. REDUCTION OF MOTOR SIZE AND WEIGHT

A. *Structure of Previously Proposed Motor*

Fig. 1 shows the 3-kW motor structure that is based on the same design concept as the previous 5-kW and 10-kW motors which were introduced in [7]-[9]. This motor structure is an internal-rotor/external-stator type in which one rotor is sandwiched by two stators, as shown in Fig. 1(a). It is difficult to generate reluctance torque effectively in the proposed motor because, as a low-cost in-wheel motor, it cannot be equipped with a powerful cooling system such as water or oil cooling. It therefore cannot conduct the high-density currents that are required to generate reluctance torque. In addition, a concentrated winding structure is used to reduce the motor size, and this is disadvantageous to generating reluctance torque. Accordingly, it is important to generate magnetic torque effectively in the proposed motor. The rotor is therefore assembled with ferrite PMs and a non-magnetic stainless steel PM holder in order to maximize magnetic torque, as shown in Fig. 1(b). We refer to this as a "coreless rotor structure".

Furthermore, the stator core shown in Fig. 1(c) is composed of soft magnetic composites [16] (SMC) that can cope with three-dimensional magnetic fluxes and that are made easily by press molding. In addition, the stator teeth are set in a simple open slot structure in order to reduce the press times and the numbers of mold templates and assembly steps.

To achieve the torque characteristics required for an electric city commuter, a reduction gearbox with a gear ratio of 10:1 is placed at one end of the stator, as shown in Fig. 1(a), and a resolver is placed at the other end. Inserting the gearbox and resolver in the dead spaces of the axial gap structure makes effective use of the limited wheel space.

B. *Problems with Miniaturization*

Table I lists the specifications and target values of the 3-kW motor. The values in Table I are the specifications of the motor alone, excluding the reduction gearbox.

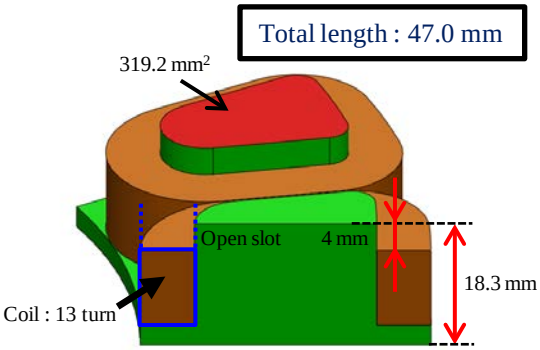

Fig. 2. Stator teeth of open slot model (A).

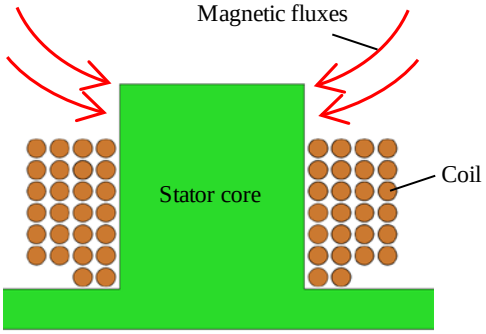

Fig. 3. Magnetic fluxes flowing into the stator core in open slot model (A).

TABLE II
MATERIAL PROPERTIES OF FERRITE PM (NMF-12G+)

Remanent magnetic flux density	0.45 T
Magnetic coercive force	-343,200 A/m
Density	5,100 kg/m^3

TABLE III
MATERIAL PROPERTIES OF SOFT MAGNETIC COMPOSITE (ML35D)

Maximum relative permeability	526
Magnetic coercive force	154 A/m
Iron loss ($W_{10/400}$)	34 W/kg
Density	7620 kg/m^3

In the proposed motor, the PM holder uses sus304 (a non-magnetic material), the ferrite PM uses NMF-12G+ (Hitachi Metal, Ltd.), and the soft magnetic composite of the stator core uses ML35D (Kobe Steel, Ltd.). Table II and III lists material properties of NMF-12G+ and ML35D.

To achieve the required specifications given in Table I, we sought a better motor shape by trials with three-dimensional finite-element analysis (3D-FEA) using the JMAG-Designer simulation software. As a result, a motor that could achieve the required specifications (e.g., output torque, speed, current density, and motor outer diameter) in Table I was designed as shown in Fig. 1. However, the axial length of this motor was 47 mm and its weight was 6.37 kg. These two size parameters could not satisfy the required specifications in Table I.

Fig. 2 shows an enlargement of two stator teeth of the motor shown in Fig. 1. We refer to the design shown in Figs. 1 and 2 as "open slot model (A)" or "open (A)." The stator teeth protrude from the upper surface of the winding area by 4 mm

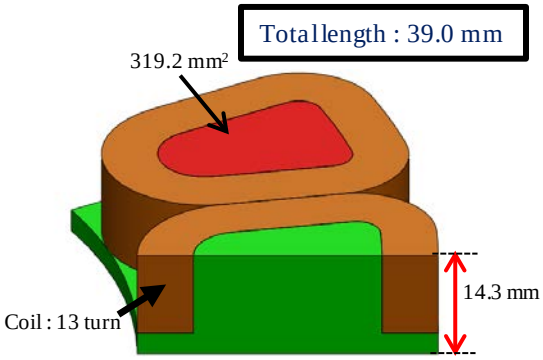

Fig. 4. Stator teeth of open slot model (B).

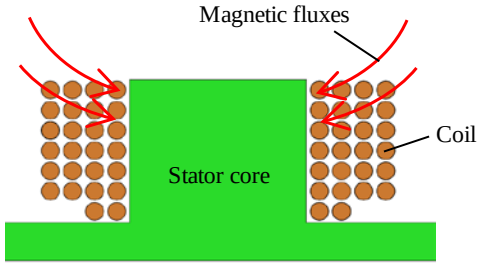

Fig. 5. Magnetic fluxes flowing into the stator core in open slot model (B).

in order to avoid the magnetic fluxes penetrating the coils directly. Fig. 3 shows a section of the open (A) stator, in which the protrusion absorbs the magnetic flux. With this structure, we expect a reduction of eddy current losses in the coils. However, these 4-mm protrusions of the stator teeth do not contribute to generating torque. They are therefore dead space from the perspective of output. Fig. 4 shows the motor which aligns the heights of the stator teeth and the winding area by reducing the each protrusion. We refer to the design shown in Fig. 4 as "open slot model (B)" or "open (B)." The total axial length of the open (B) become 39 mm, which achieves the target value in Table I. However, the magnetic fluxes now penetrate the coils directly, as shown Fig. 5, which increases the eddy current losses in the coils.

C. Relationship between Stator-tooth Protrusion and Eddy Current Loss

This section discusses the motor characteristics and the eddy current losses in the coils when the 4-mm protrusions are removed from the stator teeth.

Fig. 6 shows the 3D-FEA results for eddy current density distribution in the coils of open (A) and open (B) at the maximum speed of 5,000 rpm with no torque load. The 3D-FEA temperature of the PMs and coils is 75 °C which is target value of average motor temperature in continuous operation at maximum speed 5000 rpm. At the top of the winding area near the air gap, eddy currents arise much more in the open (B) coil than in the open (A) one.

Fig. 7 shows the 3D-FEA results for no-load eddy current losses in all coils over a whole range of rotational speed. Detailed 3D mesh models of the winding are created by using the actual winding diameter, route and number of turns. Eddy current into each winding are calculated with the detailed 3D mesh models.

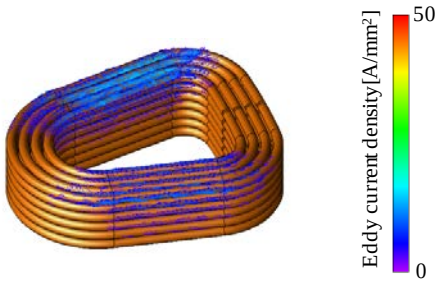

(a) Open slot model (A)

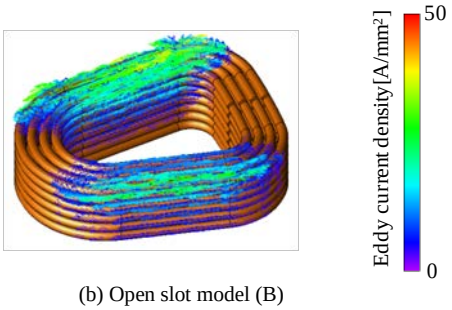

(b) Open slot model (B)

Fig. 6. Eddy current density distribution in the coil.

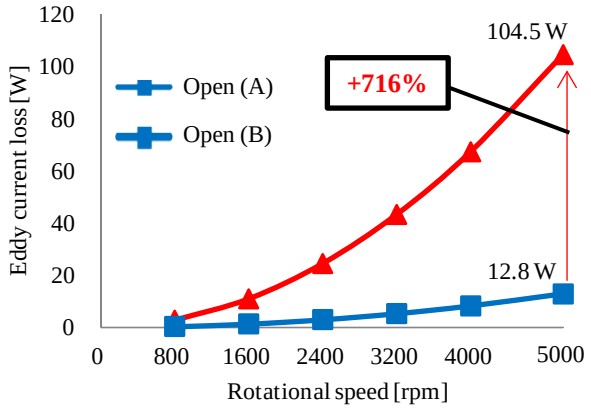

Fig. 7. Relationship between eddy current loss and rotational speed.

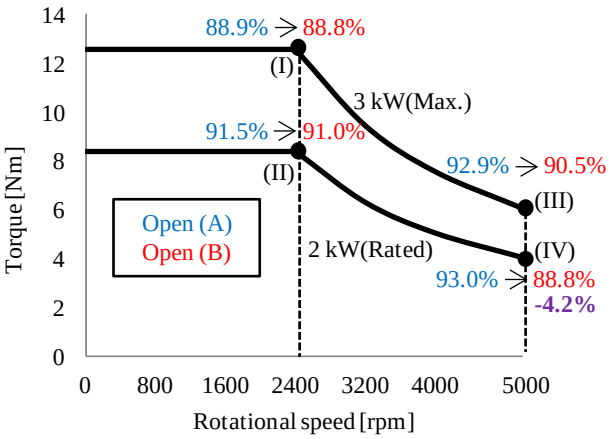

Fig. 8. Efficiencies of representative operation points in open slot model (A) and open slot model (B).

At the maximum speed of 5,000 rpm, the open (B) eddy current loss is 104.5 W, which is 8.16 times the 12.8 W of

TABLE IV
MOTOR CHARACTERISTICS OF OPEN (A) AND OPEN (B) AT REPRESENTATIVE OPERATIONAL POINTS

	(I)		(II)		(III)		(IV)	
	Open (A)	Open (B)	Open (A)	Open (B)	Open (A)	Open (B)	Open (A)	Open (B)
Rotational speed [rpm]	2400		2400		5000		5000	
Torque [Nm]	12.6	12.7	8.4	8.4	6.1	6.1	4.1	4.1
Output [W]	3167.1	3180.7	2115.8	2122.8	3187.7	3198.9	2124.7	2132.0
Total loss [W]	392.6	77.0	195.6	66.3	242.8	152.7	159.6	151.6
Copper loss [W]	322.9		143.5		180.1		100.5	
Iron loss [W]	69.7	77.0	52.1	66.3	62.7	152.7	59.1	151.6
Stator core	64.4	50.2	47.8	40.6	46.5	44.9	44.3	45.1
Coils	3.0	24.4	3.0	24.4	12.8	104.5	12.8	104.5
PM holder	2.4	2.3	1.3	1.3	3.5	3.3	2.0	2.0
Efficiency [%]	89.0	88.8	91.5	91.0	92.9	90.6	93.0	88.8

open (A). This result shows that the 4-mm protrusion from the stator teeth in the original open slot structure is very effective in reducing the eddy current loss generated in the coils.

We now discuss motor efficiency including the eddy current loss generated in the coils. Fig. 8 shows the open (A) and open (B) efficiencies at representative operational points, namely, a base speed of 2,400 rpm and a maximum speed of 5,000 rpm, and a rated output of 2 kW and a maximum output of 3 kW. Since it takes a huge amount of time to perform 3D-FEA covering the all operation area, we examine from analysis results of the above 4 representative operation points. These efficiencies are calculated simply by adding the eddy current losses generated in the coils at no load shown in Fig. 7 to the total losses of each operational point. This is because the eddy current loss cannot be analyzed under conducting currents in the simulation software that was used. At a base speed of 2,400 rpm, the efficiency reductions from open (A) to open (B) are not large. In contrast, the open (B) efficiencies are decreased notably at the maximum speed of 5,000 rpm because the eddy current loss generated in the coils increases rapidly as the speed increases, as shown in Fig. 7. For the rated output of 2 kW in particular, the efficiency decreases appreciably by 4.2%. Consequently, the open (B) efficiency is 88.8%, which is below 90% under ideal conditions. From previous experience, it is difficult to realize the continuous operation at 2 kW in an actual prototype machine.

Table IV lists the motor characteristics of open (A) and open (B) at the representative operational points (I)–(IV) shown in Fig. 8. The values of copper losses and iron losses are analysis value at each output condition. Because the current conditions are the same, there are no differences in the copper losses, whereas the iron losses are larger for open (B). At the stator core, iron losses are generated more in open (A) than in open (B) because of the stator teeth protrusion. However, the eddy current losses in the coils are much larger in open (B), so the open (B) efficiencies deteriorate at all the operational points.

D. Motor Miniaturization and Reduction of Eddy Current Loss by Adopting Semi-closed Slot Structure

The 3D-FEA results of the previous section show that it is not feasible to adopt the open slot model (B) design. Therefore,

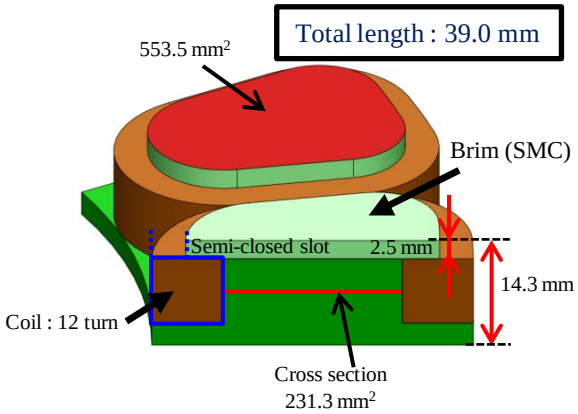

Fig. 9. Stator teeth of semi-closed slot model (C).

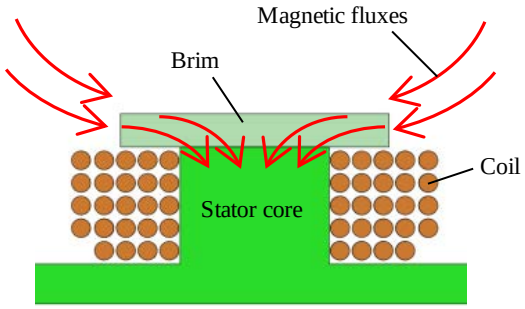

Fig. 10. Magnetic fluxes flowing into the brim and the stator core in semi-closed slot model (C).

while keeping the same axial length of 39 mm as open (B), it is necessary to reduce the eddy current loss generated in the coils. Furthermore, the open (B) weight of 5.67 kg does not achieve the target value of 5.5 kg, so it is also necessary to reduce the motor weight.

In order to solve the above problems, a semi-closed slot structure is adopted, even though this increases the production costs. Fig. 9 shows the stator teeth in the semi-closed slot structure model, now with brims of SMC arranged on top. Fig. 10 shows the new estimated magnetic flux flow. Because a larger surface facing magnets is obtained by the brims, it is possible to utilize the magnetic fluxes more effectively compared to the open slot structure. In addition, we expect a

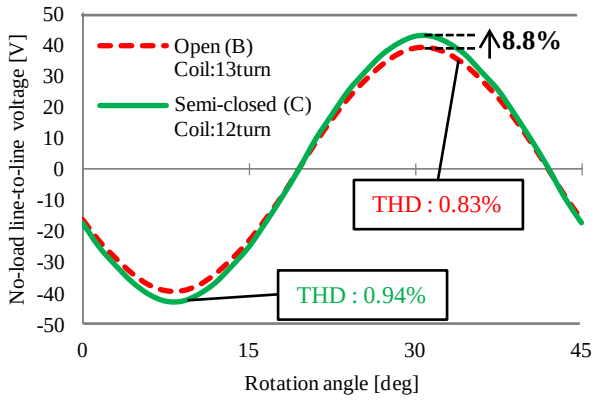

Fig. 11. Comparison of line-voltage waveform at no-torque load in open (B) and semi-closed (C).

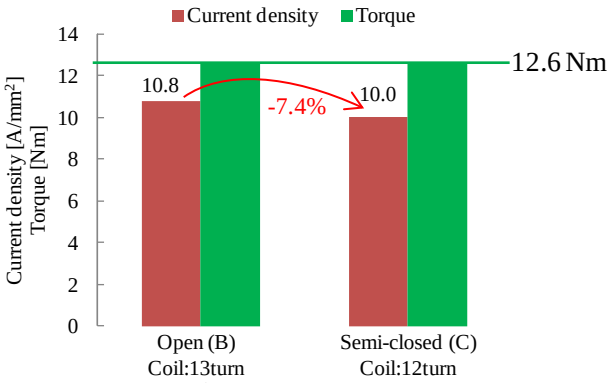

Fig. 12. Comparison of maximum current density at maximum torque in open (B) and semi-closed (C).

reduction of eddy current loss because the brims guard the coils from magnetic fluxes.

The height of the stator including the brim is 14.3 mm and the total axial length of the motor is 39 mm. These are the same values as for the open slot model (B). The shapes of the brims and stator teeth are determined by repeating 3D-FEA to achieve the required specifications in Table I. We refer to the design shown in Fig. 9 as "semi-closed slot model (C)" or "semi-closed (C)."

In semi-closed (C), the number of coil turns per stator tooth is reduced from 13 in open (B) to 12 on the condition that the fill factor is the same. To avoid decreasing the magnetic flux by reducing the coil turns, the upper surface area of the brim in the semi-closed (C) is increased from the 319.2 mm^2 of open (A) and (B) to 553.5 mm^2. Conversely, the area of the root portion of each stator tooth is decreased to 231.3 mm^2 in order to secure an area for winding the coils.

Fig. 11 shows the 3D-FEA results for line-to-line voltage waveform at no load in open (B) and semi-closed (C). Despite the reduction in coil turns, the line-to-line voltage amplitude of semi-closed (C) is 8.8% larger than that of open (B). The value of voltage per one turn of the winding at open (B) is 3.00 V/turn, and the same value at semi-closed (C) is 3.54 V/turn. The result shows that the no-load flux linkage per one turn of semi-closed (C) becomes 18.0% larger than that of open (B) by adopting the brim. In passing, both total harmonic distortions (THD) are below 1%. All models have good low-

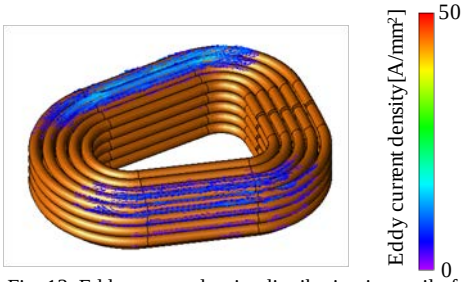

Fig. 13. Eddy current density distribution in a coil of semi-closed slot model (C).

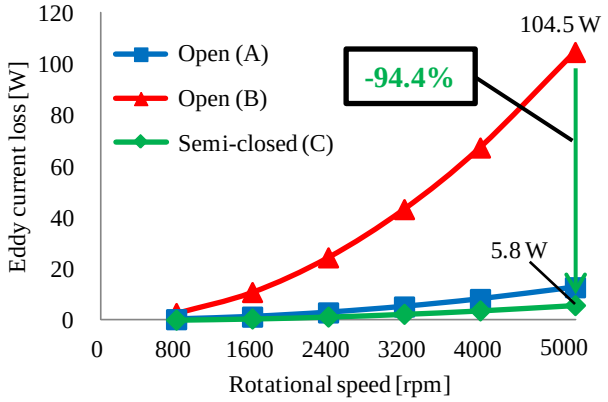

Fig. 14. Relationship between eddy current loss and rotational speed in open (A), (B), and semi-closed (C).

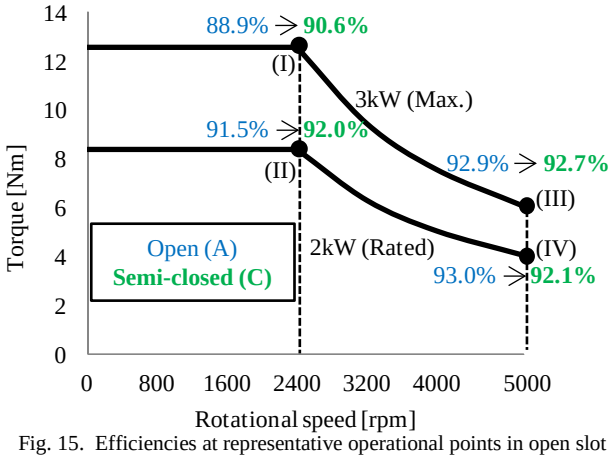

Fig. 15. Efficiencies at representative operational points in open slot model (A) and semi-closed slot model (C).

distortion characteristics because of the 16-pole/18-slot fractional-slot concentrated winding structure.

Fig. 12 shows a comparison of the maximum current density when the maximum torque of 12.6 Nm is generated. For the same generated torque, the current density of 10.0 A/mm^2 in semi-closed (C) is smaller than the 10.8 A/mm^2 in open (B).

Fig. 13 shows a 3D-FEA result for the eddy current density distribution in a semi-closed (C) coil at the maximum speed of 5,000 rpm and no torque load. The eddy current is drastically decreased from the open (B) case shown in Fig. 6(b) because the magnetic flux that penetrates the coils directly is reduced by the SMC brims.

TABLE V
MOTOR CHARACTERISTICS OF OPEN (A) AND SEMI-CLOSED (C) AT REPRESENTATIVE OPERATIONAL POINTS

	(I)		(II)		(III)		(IV)	
	Open (A)	Semi (C)	Open (A)	Semi (C)	Open (A)	Semi (C)	Open (A)	Semi (C)
Rotational speed [rpm]	2400		2400		5000		5000	
Torque [Nm]	12.6	12.7	8.4	8.5	6.1	6.2	4.1	4.1
Output [W]	3167.1	3183.2	2115.8	2141.0	3187.7	3247.6	2124.7	2165.6
Total loss [W]	392.6	308.6	195.6	167.1	242.8	205.8	159.6	145.4
Copper loss [W]	322.9	238.4	143.5	105.9	180.1	132.9	100.5	74.2
Iron loss [W]	69.7	70.2	52.1	61.1	62.7	72.9	59.1	71.2
Stator core	64.4	66.0	47.8	58.2	46.5	61.7	44.3	62.3
Coils	3.0	1.4	3.0	1.4	12.8	5.8	12.8	5.8
PM holder	2.4	2.9	1.3	1.6	3.5	5.3	2.0	3.2
Efficiency [%]	89.0	90.6	91.5	92.1	92.9	92.7	93.0	92.2

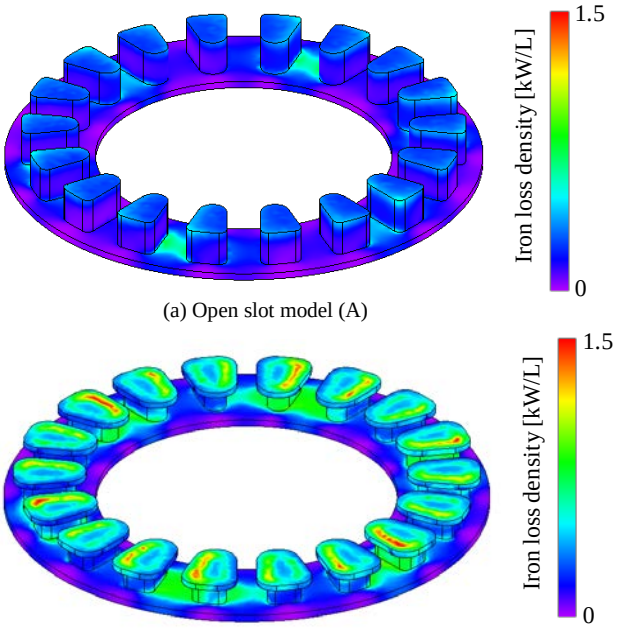

(a) Open slot model (A)

(b) Semi-closed model (C)

Fig. 16. Iron loss density distribution ofstator core at the operation point (IV).

Fig. 14 shows the 3D-FEA results for the semi-closed (C) no-load eddy current losses in all coils over a whole range of rotational speed. The results for open (A) and open (B) are also plotted for comparison. At the maximum speed of 5,000 rpm, the eddy current loss generated in semi-closed (C) is a mere 5.8 W, which is decreased by 94.4% from the open (B) loss and by 54.8% from the open (A) loss. This shows that the semi-closed slot structure is very effective in reducing the eddy current loss generated in the coils, more so than the stator-tooth protrusions in the open slot structure.

Fig. 15 shows the efficiencies at the same representative operational points as in Fig. 8 for open (A) and semi-closed (C). The efficiencies of semi-closed (C) are a little higher than those of open (A) at 2,400 rpm, and a little lower at 5,000 rpm. The former is caused by a decreased copper loss and the latter by an increased iron loss in the brims. Overall, the reduction in motor size with semi-closed (C) is sufficient to match the

TABLE VI
COMPARISON OF WEIGHT AND VOLUME IN EACH MODEL

	Open (A)	Open (B)	Semi-closed (C)
Soft magnetic core [kg]	2.23	1.88	1.83
Stator core [kg]	2.23	1.88	1.48
Brim [kg]	0	0	0.35
Coil [kg]	0.59	0.59	0.51
PM [kg]	0.54	0.54	0.54
PM holder [kg]	0.78	0.78	0.78
Total weight [kg]	6.37	5.67	**5.49**
Volume [L]	1.48	1.23	1.23

performance of the open (A).

Table V lists the motor characteristics of open (A) and semi-closed (C) at the representative operational points (I)–(IV) shown in Fig. 15. The semi-closed (C) copper losses are much lower because of decreasing the coil turns and current density, whereas its iron losses are higher. Fig. 16 shows the iron loss density distribution of the stator core at operational point (IV) in both models. Iron losses are generated constantly in the brims at high speed. For the above reasons, the semi-closed (C) efficiency is higher at low speeds; conversely, the open (A) efficiency is higher at high speeds.

Table VI gives the total weight and volume of each motor model. Open (A) exceeds open (B) and semi-closed (C) in both measures. Moreover, the semi-closed (C) stator teeth are thinner and shorter, and there are fewer coil turns. This makes semi-closed (C) lighter than open (B); at 5.49 kg, it achieves the required specification in Table I.

III. MANUFACTURE AND EXPERIMENTAL RESULTS OF PROTOTYPE

A. Manufacture of Prototype Incorporating Semi-closed Slot Structure

The simulation results above show that the semi-closed slot model (C) can achieve all the specifications in Table I. Thus, we made a prototype based on the semi-closed (C) design shown in Fig. 9. Fig. 17(a) shows a photograph of the SMC stator core with the brim. In the prototype, a segmented stator core is used to reduce production costs. The stator tooth and brim are segmented, and are made by press molding. Fig.

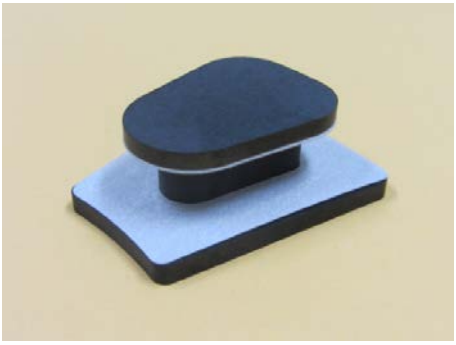

(a) Stator core

(b) Stator core (with coil)

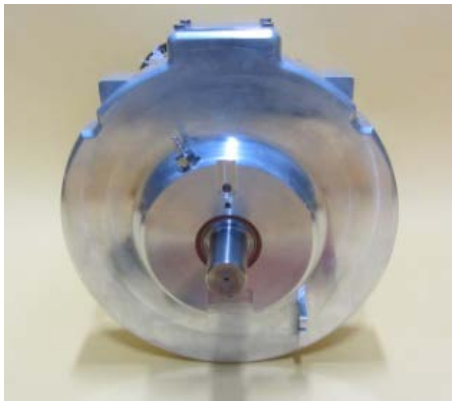

(c) Exterior

Fig. 17. Photographs of the 3-kW prototype motor.

17(b) shows the stator core wound with coils. Fig. 17(c) shows the exterior of the prototype. The weight of the prototype including its case and reduction gearbox is 11 kg.

B. Experimental Results for 3-kW Prototype Motor

The experimental test of the prototype was performed without the reduction gearbox in order to evaluate the motor characteristics alone. Furthermore, 3D-FEA is carried out with the same conditions for comparison with the experimental results. In the 3D-FEA, to consider the effect of the segmented stator core, we analyzed the non-segmented core model examined in the previous chapter and also a segmented core model with an air gap of 0.1 mm inserted between the segmented cores. Fig. 18 shows a section of the segmented-stator-core analysis model. The 0.1-mm air gaps are placed

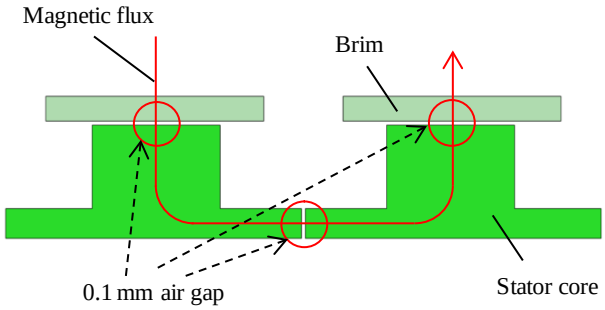

Fig. 18. Analysis model of segmented stator core.

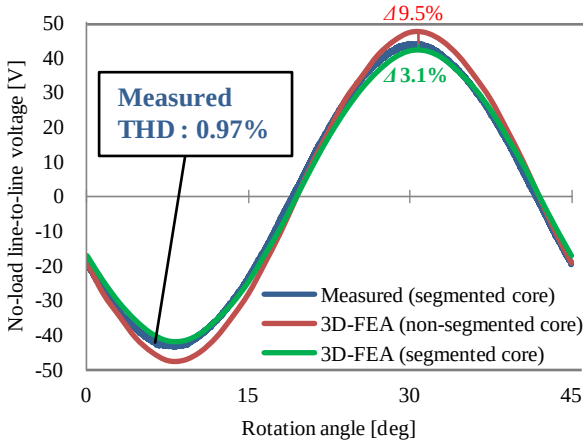

Fig. 19. Comparison of line-to-line voltage waveform at no-torque load in experimental test and 3D-FEA at prototype.

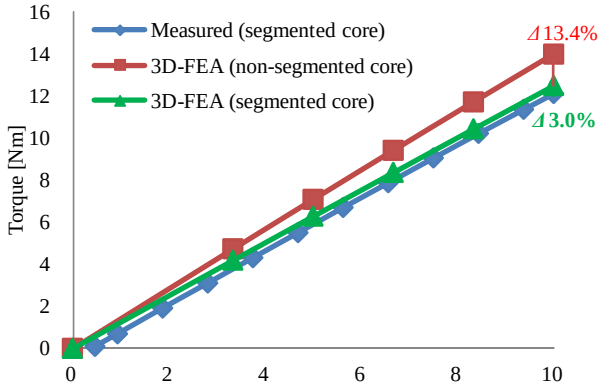

Fig. 20. Comparison of torque characteristics in experimental test and 3D-FEA for prototype.

between the back yokes and between the brims and the stator teeth.

Fig. 19 shows the line-to-line voltage waveform at no load. The line-to-line voltage amplitude of the experimental result is 9.5% smaller than the analysis result for the non-segmented core model. In contrast, the difference compared to the analysis result for the segmented core model is only 3.1%.

Fig. 20 shows the relationship between torque and current density. The prototype can achieve 12 Nm, which is the target value given in Table I. The experimental results for the prototype agree well with the analysis results for the

segmented core model.

The results of Fig. 19 and Fig. 20 show that the magnetic resistance increases in air gaps between segmented cores. Therefore, the air-gap magnetic flux density between rotor and stator decreases, hence the voltage decreases as shown Fig. 19 and the torque decreases as shown Fig. 20. It is possible to evaluate the effect of the segmented stator core by means of 3D-FEA.

Fig. 21 shows the efficiency map of the prototype. This was obtained by correcting for machine loss, which is measured by using the non-magnetized rotor. The maximum efficiency is 93.3% at 3,200 rpm, and high efficiencies over 90% are realized over a wide range. Moreover, a constant power output of 3 kW is accomplished at rotational speeds of 2,400–5,000 rpm.

Fig. 22 shows the changes in coil temperature at a base speed of 2,400 rpm or the maximum speed of 5,000 rpm, and for a rated output of 2 kW or the maximum output of 3 kW. Although the winding temperatures at the maximum output of 3 kW rise to 90 °C, this takes 15 min 5 s at 2,400 rpm and 17 min 37 s at 5,000 rpm. This confirms that the proposed motor would have sufficient time to accelerate in a city commuter. The winding temperature for the rated output of 2 kW at 2,400 rpm reaches a balance at 92.2 °C. Similarly, the winding temperature for the rated output of 2 kW at 5,000 rpm reaches a balance at 78.4 °C. At any speed, continuous operation at 2 kW is available from the prototype.

From all our experimental results, the 3-kW prototype motor achieves all required specifications in Table I.

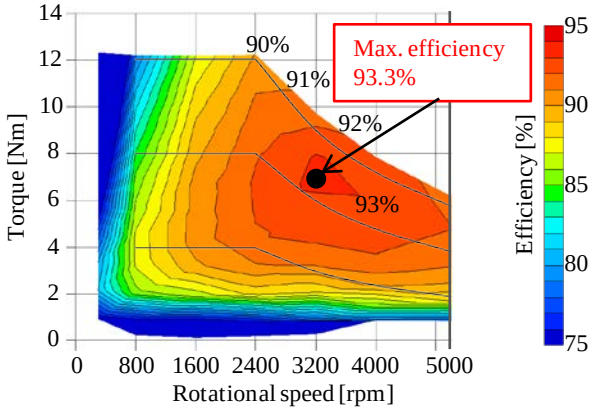

Fig. 21. Efficiency map of the 3-kW prototype motor.

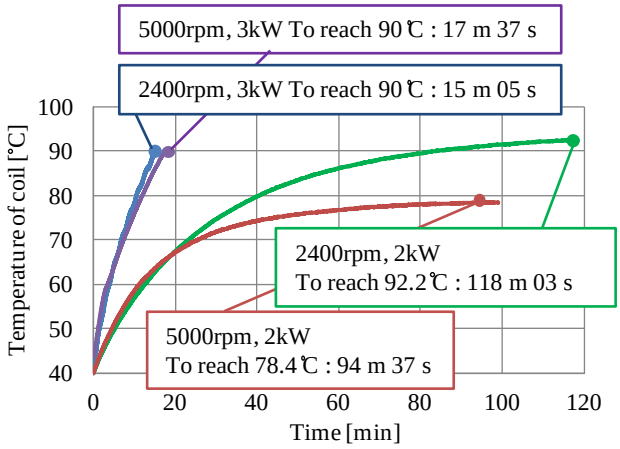

Fig. 22. Temperature of the winding in the 3 kW prototype motor.

IV. Conclusion

To reduce the size and weight of a 3-kW in-wheel axial-gap motor with ferrite permanent magnets that is intended for electric commuter cars, we examined the adoption of a semi-closed slot structure instead of an open slot structure. The analysis results of 3D-FEA showed that the semi-closed slot structure, in which SMC brims are attached to the tops of the stator teeth, could give a smaller size and weight than those of the conventional open slot structure. The efficiency of the proposed motor was maintained despite the miniaturization. Furthermore, we confirmed experimentally that a prototype motor could fulfill all the required specifications for an electric city commuter.

References

[1] H. Yashiro, I. Miki, K. Yamamoto, "A study on performance optimization for switched reluctance motors designed for commuter-type electric vehicles",in Proceedings of the 16th International Conference on Electrical Machines and Systems (ICEMS 2013), Oct. 2013

[2] Wei Hua, Hengliang Zhang, Ming Cheng, Jianjian Meng, Chuang Hou, "An Outer-Rotor Flux-Switching Permanent-Magnet-Machine With Wedge-Shaped Magnets for In-Wheel Light Traction", IEEE Trans. Industrial Electronics, vol. 64, issue 1, Jan 2017

[3] Shi-Uk Chung, Seok-Hwan Moon, Dong-Jun Kim, Jong-Moo Kim, "Development of a 20-Pole–24-Slot SPMSM With Consequent Pole Rotor for In-Wheel Direct Drive", IEEE Trans. Industrial Electronics, vol. 63, issue 1, Jan 2016

[4] Jianing Lin, Nigel Schofield, Ali Emadi, "External-Rotor 6−10 Switched Reluctance Motor for an Electric Bicycle", IEEE Trans. Transportation Electrification, vol. 1, issue: 4, Dec 2015

[5] C. Versele, Z. De Greve, F. Vallee, R. Hanuise, O. Deblecker, M. Delhaye, and J. Lobry, “Analytical design of an axial flux permanent magnet in-wheel synchronous motor for electric vehicle”, in Proc. of 13th European Conference on Power Electronics and Applications (EPE '09), 9 pages (CD-ROM), Sept. 2009.

[6] M. Aydin, S. Huang, and T. A. Lipo “Torque Quality and Comparison of Internal and External Rotor Axial Flux Surface-Magnet Disc Machines”, IEEE Trans. Ind. Electronics, Vol. 53, No. 3, pp. 822-830, June 2006.

[7] K. Sone, M. Takemoto, S. Ogasawara, K Takezaki, and H Akiyama, “A Ferrite PM In-Wheel Motor without Rare Earth Materials for Electric City Commuters”, IEEE Trans. Magn., vol. 48, no. 11,pp. 2961–2964, Nov. 2012.

[8] K. Sone, M. Takemoto, S. Ogasawara, K. Takezaki, and W. Hino, “Operation Characteristics of Ferrite Permanent Magnet In-Wheel Axial-Gap Motor with Coreless Rotor Structure for Electric City Commuters,” in Proc. of the 2013 IEEE Energy Conversion Congress and Exposition (ECCE 2013), pp. 3186-3193, 2013.

[9] K. Sone, M. Takemoto, S. Ogasawara, K. Takezaki, and W. Hino, “Examination for the Higher Efficiency in a Ferrite Permanent Magnet 10 kW In-Wheel Axial-Gap Motor with Coreless Rotor Structure”, in Proc. of the 2014 IEEE Energy Conversion Congress and Exposition (ECCE 2014), pp. 5885-5892, 2014.

[10] Sung Chul Oh and A Emadi, “Test and simulation of axial flux-motor characteristics for hybrid electric vehicles”, IEEE Trans. Vehicular Technology, vol. 53, no. 3, pp. 912-919, May 2004.

[11] M. Aydin, S. Huang, and T.A. Lipo, “Axial Flux Permanent Magnet DiscMachines: A Review”, in Conf. Record of SPEEDAM, pp. 61-71, May 2004.

[12] K. M. Rahman, N. R. Patel, T. G. Ward, J. M. Nagashima, F. Caricchi, and F. Crescimbini, “Application of direct-drive wheel motor for fuel cell electric and hybrid electric vehicle propulsion system,” IEEE Trans. Ind. Applicat., vol. 42, no. 5, pp. 1185–1192, Sep./Oct. 2006.
[13] T. J. Woolmer and M. D. McCulloch, “Analysis of the Yokeless And Segmented Armature Machine”, in Proc. 2007 IEEE Int. Electric Machines and Drives Conf. (IEMDC2007), pp.704-708, 2007.
[14] Y.-P. Yang and D. S. Chuang, “Optimal design and control of a wheel motor for electric passenger cars,” IEEE Trans. Magn., vol. 43, no. 1,pp. 51–61, Jan. 2007.
[15] S. Javadi, and M. Mirsalim, “A Coreless Axial-Flux Permanent-Magnet Generator for Automotive Applications”, IEEE Trans. on Magn., Vol. 44, No. 12, pp. 4591-4598, DEC. 2008.
[16] N. Bianchi, S. Bolognani, P. Frare, “Design criteria of high efficiency SPM synchronous motors”, Electric Machines and Drives Conference 2003 (IEMDC 03), 2003
[17] T. Takahashi, M. Takemoto, S. Ogasawara, W. Hino and K. Takezaki, “Size and Weight Reduction of an In-Wheel Axial-Gap Motor Using Ferrite Permanent Magnets for Electric City Commuters”, in Proceedings of the 18th International Conference on Electrical Machines and Systems (ICEMS 2015), Oct. 2015.

Tomohira Takahashi was born in Sapporo, Japan, in 1991. He received the B.S. and M. S. degree from the Graduate School of Information Science and Technology, Hokkaido University, Sapporo, Japan, in 2014 and 2016, respectively.

He is engaged in research on axial gap motors using ferrite permanent magnets.

Mr. Takahashi is a member of IEEE and the Institute of Electrical Engineers of Japan (IEEJ).

Masatsugu Takemoto (M’99) was born in Tokyo, Japan, in 1972. He received the B.S. and M.S. degrees in electrical engineering from Tokyo University of Science, Noda, Japan, in 1997 and 1999, respectively, and the Ph.D. degree in electrical engineering from Tokyo Institute of Technology, Tokyo, in 2005. In 1999, he joined Tokyo Institute of Technology as a Research Associate in the Department of Electrical Engineering. In 2004, he joined Musashi Institute of Technology, Tokyo, as a Research Associate in the Department of Mechanical Systems Engineering, where he became a Lecturer in 2005. Since 2008, he has been with Hokkaido University, Sapporo, Japan, where he is an Associate Professor in the Division of Systems Science and Informatics. He is engaged in research on permanent magnet synchronous motors, axial gap motors, rare-earth-free motors, bearingless motors, and magnetic bearings.

Dr. Takemoto is a member of the Institute of Electrical Engineers of Japan (IEEJ). He was the recipient of IEEJ Transaction Paper Award in 2005. He has served as Secretary, Vice-Chair, and Chair of the IEEE IAS Japan chapter in 2008–2009, 2010–2011, and 2012-2013, respectively**.**

Satoshi Ogasawara (A’87–M’93–SM’97) was born in Kagawa, Japan, in 1958. He received the B.S., M.S., and Dr. Eng. degrees in electrical engineering from the Nagaoka University of Technology, Niigata, Japan, in 1981, 1983, and 1990, respectively. From 1983 to 1992, he was a Research Associate with the Nagaoka University of Technology. From 1992 to 2003, he has with the Department of Electrical Engineering, Okayama University, Okayama, Japan. From 2003 to 2007, he was with the Department of Electrical Engineering, Utsunomiya University, Utsunomiya, Japan. Since 2007, he has been a Professor in Graduate School of Information Science and Technology, Hokkaido University, Sapporo, Japan. His research interests include ac motor drive systems and static power converters.

Dr. Ogasawara received the IEEE/PELS Society Prize Paper Award in 1999, and the IEEE/IAS Committee Prize Paper Awards in 1996, 1997, 2003, and 2010. He is a Senior Member of the Institute of Electrical Engineers of Japan.

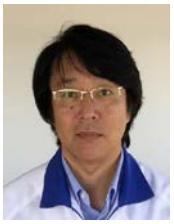

Kenichi Takezaki was born in Chitose, Japan, in 1962. He received the B.S. degree from the Faculty of Fisheries, Hokkaido University, Hakkodate, Japan, in 1986.

Since 1986, he has been with Development Headquarters, Dynax Corp., Chitose, Japan.

He is engaged in research on axial gap motors using ferrite permanent magnets.

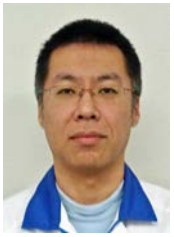

Wataru Hino was born in Oshamanbe, Japan, in 1971. He received the B.S. degree from the school of Engineering, Hokkaido University, Sapporo, Japan, in 1995. Since 1998, he has been with Development Headquarters, Dynax Corp., Tomakomai, Japan.

He is engaged in research on axial gap motors using ferrite permanent magnets.